LPG interrogator based on FBG array and Artificial Neural Network

Felipe O. Barino and Alexandre Bessa dos Santos

***Abstract*—This work introduces a new method for long-period fiber grating (LPG) sensors interrogation. This proposal uses a fiber Bragg grating (FBG) array to extract spectral information of the LPG sensor and an Artificial Neural Network to process this information. The information is processed to estimate the LPG resonant wavelength, without prior knowledge on the LPG spectrum. Therefore, the interrogator is LPG-insensitive, can be easily manufactured by optical fiber sensors laboratories at low-cost and is suitable for in-field applications. We demonstrated the filter array and Multilayer Perceptron (MLP) design, which are the proposed interrogator core. Furthermore, we analyzed the interrogation performance by the Mean Squared Error (MSE), the Mean Absolute Error (MAE), and the distribution of the residuals. The results showed our proposal can estimate the LPG resonant wavelength with 2.82 nm uncertainty, considering a 95% confidence interval, over 75 nm dynamic range for several LPGs, with different spectral characteristics. Moreover, our proposal can be easily tailored for different dynamic ranges and resolutions with proper adjustments on the FBG array and MLP.**

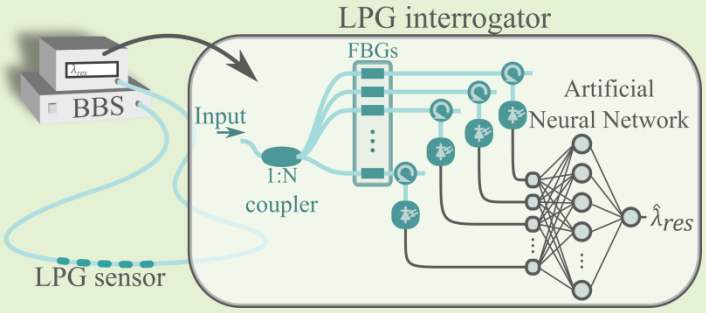

***Index Terms*— long-period fiber gratings, optical fiber sensor, interrogation, artificial neural network, machine learning**

I. Introduction

ADVANCES in optical communication market have been favorable to optical fiber sensor technology, due to the large number of suppliers and the increase in optical components offer at a good cost benefit [1]. The fiber Bragg gratings (FBGs) and long-period fiber gratings (LPGs, or LPFGs) are two important structures in optical fiber sensing. Both are in-fiber passive devices based on diffraction gratings, which are manufactured by periodic modulation of fiber's properties.

LPGs are easier to manufacture, when comparing to FBGs, due to its longer modulation period and can be easily made using point-by-point techniques. An example of an easy and low-cost manufacturing technique for LPGs is the arc-electric technique, for example [2].

Fiber diffraction gratings couple light between waveguide's propagation modes, in LPGs this coupling occurs between the fundamental core mode and an evanescent cladding mode. The energy coupled to this cladding mode is rapidly attenuated due to scattering of light at the cladding/external medium interface [3], [4]. Therefore, an LPG transfer function is a notch filter centered at the wavelength which modes were coupled, by the LPG phase-matching condition, this wavelength is:

$$\lambda_{res}^{m} = \left(n_{eff,co} - n_{eff,cl}^{m}\right)\Lambda \qquad (1)$$

where $n_{eff,co}$ and $n_{\mathrm{eff,cl}}$ are, respectively, the core and cladding effective index, Λ the grating period, λ_{res} is the resonant wavelength and m denotes the coupling order.

LPGs can be used as sensors because the resonant wavelength is a function of parameters that changes with the surrounding refractive index (SRI), mechanical deformation, and temperature [5]. $n_{eff,co}$ and $n_{\mathrm{eff,cl}}$ changes due to photo-elastic and termo-optic effect; $n_{\mathrm{eff,cl}}$ due to cladding/external medium interface; and Λ changes with thermal expansion and mechanical deformation.

Therefore, the measurement is a function of LPG's resonant wavelength and we have to correlate the measurement to this resonant wavelength in order to use the LPG as a sensor. This process is called interrogation and most of the methods reported in the literature require expensive and/or bulky equipment.

Due to LPGs large full width at half maximum (FWHM), they are hard to perform in-field interrogation and generally, its interrogation consists of illuminating the LPG with a broadband light source, obtain the spectrum with an optical spectrum analyzer (OSA), and identify the resonant wavelength. Another interrogation technique uses wavelength-swept lasers to identify the resonant wavelength [6], [7]. Both approaches search for λ_{res}^{m} in a large spectral range; therefore, these approaches can be used for a wide range of LPGs. A

This work was supported by the PBPG-UFJF, CNPq, CAPES, Inerge-UFJF, and Santo Antônio Energia.

F. O. Barino is with the Programa de Pós-Graduação em Engenharia Elétrica (PPEE-UFJF) at Federal University of Juiz de Fora, Juiz de Fora, 36036-900, Brazil (e-mail: felipe.barino@engenharia.ufjf.br).

A. B. dos Santos is with the Department of Circuits, Federal University of Juiz de Fora, Juiz de Fora, 36036-900, Brazil (e-mail: alexandre.bessa@engenharia.ufjf.br).

cheaper and more compact solution is to design optical filters close to the LPG resonant wavelength and correlate the optical power filtered with the measurement [8]-[11].

Although these interrogators based on optical filtering techniques are cheap, they are often tailored to a single sensor. In these cases, the sensing and interrogation systems are coupled, because the filters need to be optimally designed for a single LPG. To overcome this drawback, [12] proposed an interrogation system based on temperature-modulated arrayed waveguide gratings (AWG), this interrogator was able to recover the LPG spectrum using several power measurements made by the modulated AWG channels. The authors reported that the system can determine the LPG resonant wavelength with 1 pm resolution over a 25 nm dynamic range. But the AWG is still an expensive device to be used in a single LPG interrogation and some laboratories that work with optical fiber sensors don't have access to the integrated-photonics manufacturing process. Recently [13] has presented a simpler and cheaper solution, low-cost LPG interrogator using three temperature modulated lasers that adjust an LPG spectrum to the optical power scanned by the modulated laser array. Although they reported that the same fitting function could be used for different LPGs, the parameters of this function needed to be optimized for each LPG.

This study proposes a new approach to filter-based LPG interrogation; this approach maintains the low-cost of traditional filter-based interrogators adding the generalization capability of more complex interrogation systems. The proposed interrogator uses an array of FBG filters to estimate the LPG resonant wavelength by an artificial neural network (ANN), a multilayer perceptron (MLP).

The use of ANN in LPG based optical sensors as a spectral processing tool is well described in the literature. In general, spectral features are extracted and then fed into the neural network to obtain the measurement. In [14] two LPGs were used alongside an MLP to measure temperature and curvature; in [15] another LPG-ANN-based multi-parameter sensor was designed to temperature and deformation discrimination; on the other hand [16] used different spectral features of a single LPG as the input of an ANN to estimate the fiber curvature; while [17] compared multiple machine-learning-based regression techniques, including ANNs, in 2D load measurement using a single LPG; for refractive index measurements, [18] demonstrated an LPG-ANN-based classifier and its application in the fuel industry. Recently, [19] presented an adaptive-network-based fuzzy inference system (ANFIS) to boost LPG strain sensor accuracy using the LPG resonant wavelength and the attenuation data as the ANFIS input.

Machine learning has also been used in other types of optical fiber sensors such as FBGs embedded in the pavement for vehicle classification using support vector machine [20], an ANN ensemble was also reported to process data from four FBGs to estimate impact location in structures [21], and novel deep learning techniques were also employed in detection and location of human walking by using generative adversarial networks to process distributed acoustic sensing data [22]. In contrast to our work, in [23] the authors reported on FBG interrogation using a pair of LPG and an ANN to estimate the location and intensity of strain applied to an FBG pair. We chose to work with LPGs as sensors due to its increased sensitivity (to both strain and temperature) and the ability to measure SRI without coating the fiber. This high sensitivity could introduce random fluctuations and wrong measurements due to cross-sensitivity, but several methods were reported to overcome these problems [24]-[26]. Moreover, the literature lacks simple and low-cost LPG interrogation techniques for in-field use that have the same level of generalization as presented here; to our knowledge, a similar approach to LPG interrogation is only addressed in [13].

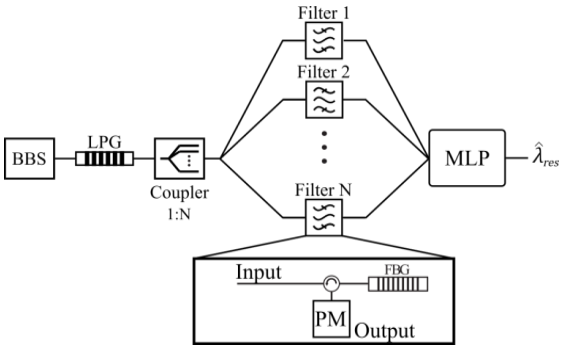

Fig. 1. Illustration of the proposed interrogation scheme. A BBS source is used to illuminate the interrogating LPG sensor, while the proposed interrogator is used to estimate its resonant wavelength ($\hat{\lambda}_{res}$).

Furthermore, most works on ANN-based LPG systems used spectral features extracted by some sort of interrogation system, typically an OSA, as ANN input. The most used features are the resonant wavelength and the resonant dip attenuation, for one or more transmission dip. Additionally, the works on interrogation techniques focus more on specific sensors, thereof the interrogator is usually coupled to the sensor itself. Nevertheless, our interrogator uses features extracted by N filters and outputs the LPG resonant wavelength, regardless of the measure or LPG itself. This way, the interrogation system is generic and completely decoupled from the LPG. The scheme for our proposal can be seen in Fig. 1.

Therefore, this new interrogator brings the flexibility of spectrum-based interrogation and the low-cost of filter-based interrogation. Although the FBG array channels are sparse, when compared to an AWG, they don't require expensive integrated-photonics manufacturing process. The cost of optical components might be around tenths the cost of an OSA, depending on the number of FBG modules used. Moreover, laboratories that work with LPGs and other types of optical fiber sensors usually manufacture FBGs; therefore, these laboratories can easily manufacture the proposed interrogator for their LPG sensors with reduced cost.

II. Methods

The optical setup for the LPG interrogator is composed of a 1xN optical splitter, N optical circulators, N FBGs, and N photodiodes, as illustrated in Fig. 1. This configuration forms an array of optical power measurements of the LPG spectrum filtered by the FBG array. The FBG array data processing is the interrogator principal component and we choose ANNs because they are computational models capable of mapping an

input set of features into an output space using knowledge acquired during a training procedure [27], [28]. Furthermore, ANN's characteristics like memory and generalization are crucial characteristics of our LPG interrogation scheme. Due to sparse filtering, the data processing system needs to know the general characteristics of an LPG transmission spectrum and infer the resonant wavelength position using little data. In other words, the ANN uses its memory to interpolate the points filtered by the FBGs and estimate the resonant wavelength position.

There are a great number of topologies and algorithms for ANNs and among them, we can highlight the MLP as an important structure for nonlinear regression, since it is capable of approximating any function with a finite number of discontinuities with only one hidden layer [29].

An MLP has at least three layers: an input layer, $N_e > 1$ hidden layer(s), and one output layer. The nodes of these layers are connected by weights, named synaptic weights, and these nodes are called neurons (except for the input layer). We used a three-layer perceptron in this study, as the one shown in Fig. 2.

During training, a set of input/output pairs are shown to the MLP and the synaptic weights, represented by $w_{n,a}$ in Fig. 2, are updated to reduce the error between model estimation and the real output [27], [28]. The subscript n and a denotes the final node and the initial node that the weight $w_{n,a}$ connects.

The MLP illustrated in Fig. 2 processes the input data as follows: the N inputs are passed to the hidden layer and each hidden neuron processes this data by a linear combination with its weights and a bias is added to the result; finally, this result is fed into the neuron activation function $f(\cdot)$ that results in the neuron output. Therefore, let h_i be the i^{th} hidden layer neuron output, x_k the k^{th} neural network input, and b_i the neuron bias; the hidden layer output is given by:

$$h_i = f\left(b_i + \sum_{k=0}^{N-1} x_k w_{i,k}\right), \forall\, i \in \{0, \ldots, H-1\} \quad (2)$$

where H is the hidden layer size. Finally, the hidden layer output is fed into the output neuron to return the MLP estimative:

$$y = b_y + \sum_{i=0}^{H-1} h_i w_{y,i} \quad (3)$$

where b_y is the output neuron bias and $w_{y,i}$ the synaptic weight connecting the h_i neuron output to the output neuron y. Note that there is no activation function in equation (3) since the output y needs to be real-valued, in order to perform function approximation.

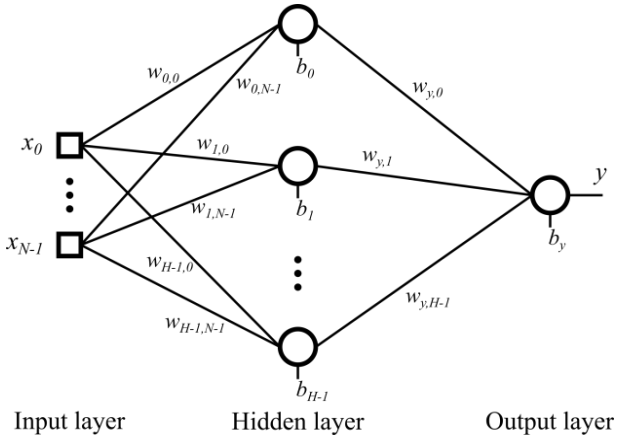

Fig. 2. N input by one output MLP scheme. Input nodes are shown in squares, neurons in circles and synaptic weights are represented by the lines joining them.

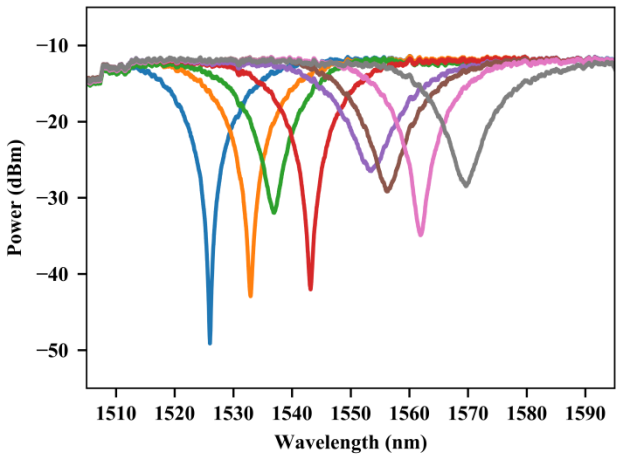

Fig. 3. Spectrum of eight randomly chosen LPGs from the database.

To design and evaluate this MLP a set of 528 spectra containing a single peak of 83 different arc-induced LPGs was used, they were fabricated using different grating periods and electric arc configurations. These LPGs have a wide variety of spectral characteristics like full width at half maximum (FWHM), resonant wavelength, attenuation intensity, and different attenuation dip asymmetries. Furthermore, the 83 LPGs were submitted to different temperature and mechanical stress, adding up to a total of 528 spectral curves; eight samples of these curves were randomly chosen and can be seen in Fig. 3. Moreover, the resonant wavelength, FWHM, and attenuation intensity for these 528 spectra are summarized in Fig. 4, where the LPG period (Λ) is represented by different symbols. Note that for each grating period several LPGs were manufactured using different electric arc intensities, which are represented by the different colors. Hence, one can see the great variability presented by the spectra used that could guarantee the trained ANN good generalization.

We split the dataset randomly into three parts: train (60%), test (20%), and validation (20%). The train set was used to train MLP models in different scenarios (several hidden layer configurations), while the validation set was used to evaluate

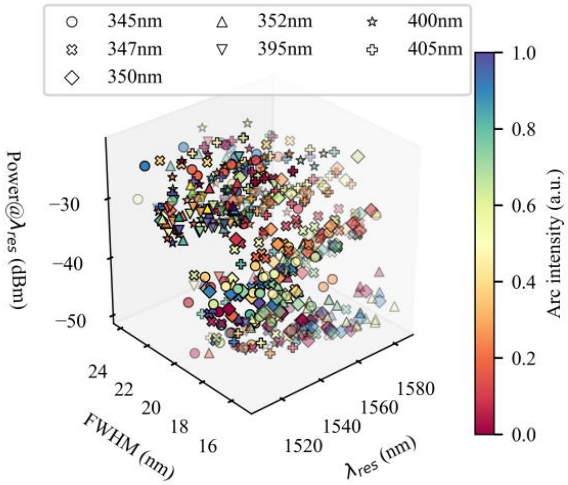

Fig. 4. Spectral features of all spectra used in this work.

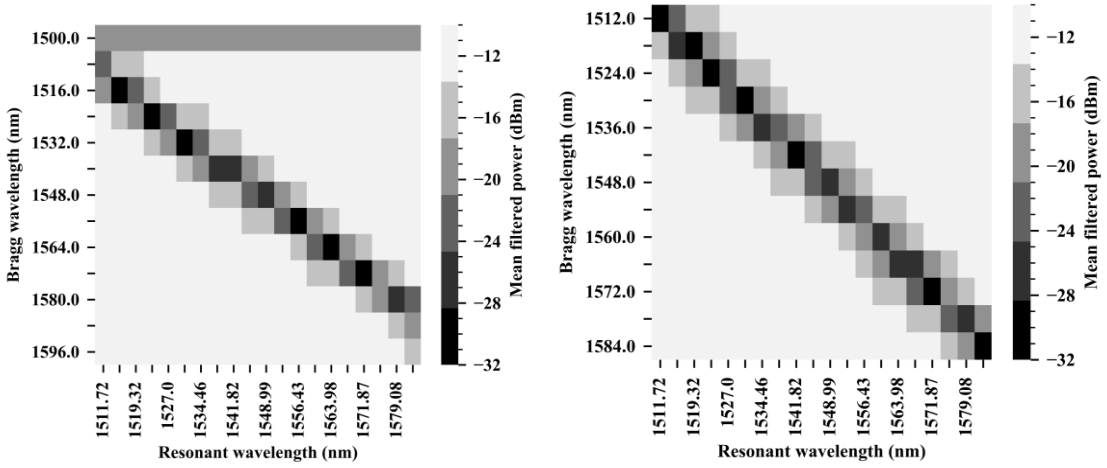

(a) 1500 nm-1596 nm array (b) 1512 nm-1584 nm array

Fig. 5. Relationship between filtered power by each FBG and the LPG resonant wavelength for the (a) 1500 nm – 1596 nm array and (b) 1512 nm – 1584 nm FBG array.

these trained models and select the best one as the final MLP for the interrogator. Lastly, the test set was used after model selection to evaluate the interrogator performance.

In our MLP design, feature selection is simply designing the filter array, since its power measurements were used as MLP inputs. Hence, the number of FBGs and their spacing in wavelength domain were the central points of this design. Furthermore, we analyzed the spectral characteristics using the test and validation data, leaving the test data only for evaluating the final design. We focused on the minimum and maximum resonant wavelength as well as the mean and minimum FWHM to choose a good FBG array configuration.

While we used the resonant wavelength information to determine the maximum and minimum detectable λ_{res}, the FWHM gives information about the FBG spacing. The right FBG array density is crucial to perform resonant wavelength detection. By choosing the correct FBG spacing we can ensure that at least one filter is in the LPG's dip region. In this case, the distance between the two filters needs to be at least half the LPG's FWHM. Indeed, one can see that the worst-case scenario is when two FBGs are at the LPG's -3 dB transmission spectrum points. If we add a third filter at the mean of these previous two filters, it is within the LPG rejection band and the spacing is half of FWHM. In this case, if the LPG's resonant wavelength moves, two FBGs will be at the LPG rejection band. Moreover, the more FBGs are added in between, more information about the LPG rejection band is extracted and we expect that better resonant wavelength estimation could be obtained.

After the filter array design, we collected the optical power for every spectrum using the designed FBG array and normalize this data to the $[0,1]$ interval, obtaining input/output pairs for MLP development. Moreover, we choose the MLP hidden layer size by trial and error over different configurations. In all cases, we used ReLU (Rectified Linear Unit) activation function at the hidden layer neurons, whereas the weights were optimized to reduce the mean squared error (MSE) by the LBFGS method using early stopping with patience of 12 iterations. Since early stopping would prevent overfitting, we set the maximum iteration parameter as high as 10000.The whole process was made in python using the scikit-learn library [30], note that all remaining parameters not cited in this paper were kept as the library default.

The trial and error model selection was made by training and validating 20 times the same architecture, which varied from 3 to 8 neurons at the hidden layer ($N_e \in \{3, 4, \dots, 8\}$). We select the model based on a trade-off between the minimum validation MSE and its variance over the 20 times we trained the model.

After the final model was selected, we performed the model evaluation at the test set by the MSE in λ_{res} estimation, the mean absolute error (MAE), and residual analysis. Furthermore, we visualize the interrogator output by a curve relating the observed λ_{res} to the estimated λ_{res}.

Lastly, we used the proposed interrogator to characterize a 340 µm period LPG for SRI using different concentrations of Ethylene glycol with RI from 1.000 RIU (air) to 1.429 RIU (100% Ethylene glycol). This LPG was not part of the initial database, to simulate an in-field application of the proposed interrogator.

III. Results

Analysis of the spectra showed resonant wavelengths available by the dataset are located between 1510 nm and 1585 nm, while the mean FWHM is 18.64 nm and its minimum value is 15.30 nm.

Therefore, we evaluated an FBG array from 1500 nm to 1596 nm with 8 nm between the filters. This array covered all resonant wavelengths in our dataset and guaranteed that at least one FBG filter was at the LPG dip for the most sensors used. The FBG array evaluation was made by analyzing the relationship between the LPG resonant wavelength and the filtered data for every FBG. We separated the LPGs resonant wavelengths in 20 equally spaced regions, similarly to histogram bins. For each resonant wavelength region, we calculated the mean filtered power by each FBG and plotted the result in a color map. This graph is shown in Fig. 5, the x-axis represents the LPG resonant wavelength section and the y-axis the Bragg wavelength of each FBG. Color intensity

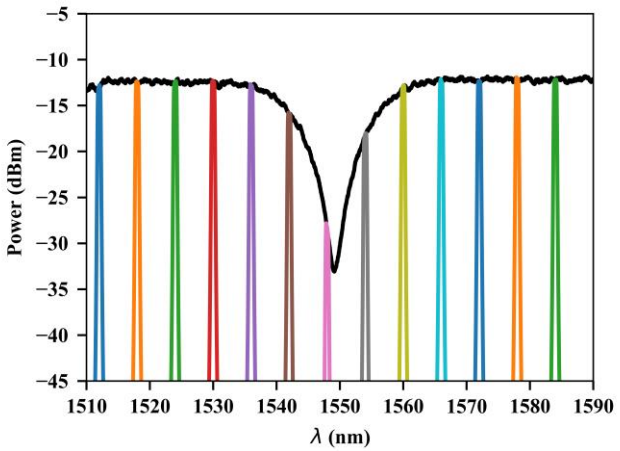

Fig. 6. LPG transmission spectra and the filtered results by the designed FBG array.

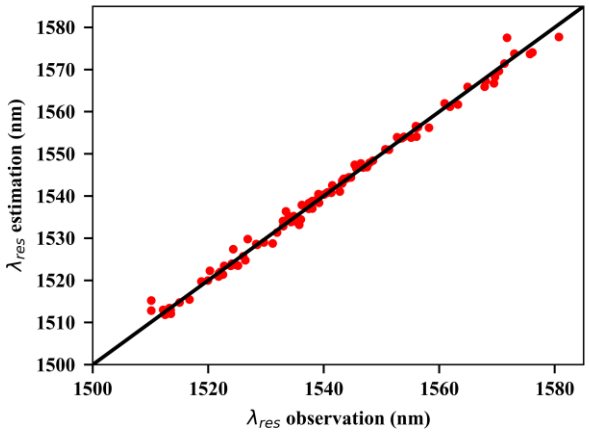

Fig. 8. Observed vs estimated resonant wavelength.

represents the mean filtered power by the FBG at each resonant wavelength section.

One can see in Fig. 5a that for the 1500 nm – 1596 nm array, the optical power filtered by FBGs at 1500 nm, 1508 nm, 1588 nm, and 1596 nm presents low variation concerning λ_{res}. Therefore, these FBGs acquired little or no information about the LPG resonant wavelength and can be removed or adjusted. Consequently, we adjust the FBG array to 1512 nm – 1584 nm, now spaced by 6 nm. We reduce the window size from 1500 nm – 1596 nm to 1512 nm – 1584 nm because FBGs at 1500 nm and 1596 nm had power variation close to zero in the first array. At the same time, the minimum filtered values of FBGs at 1508 nm and 1588 nm were higher than any other FBG; hence, these FBGs did not inform as much about the LPG resonant wavelength as the others.

Therefore, we reduced the window to a range where there is greater power variation at the FBG array relative to the LPG resonant wavelength. This new array is more conservative with respect to the FBG spacing than the previous FBG array. The resulting relationship between LPGs resonant wavelength and filtered power by the new FBG array can be seen in Fig. 5b, where one can see that the filtered power is more equally distributed along the resonant wavelength, note the perfect diagonal formed by lower values of mean filtered power. This

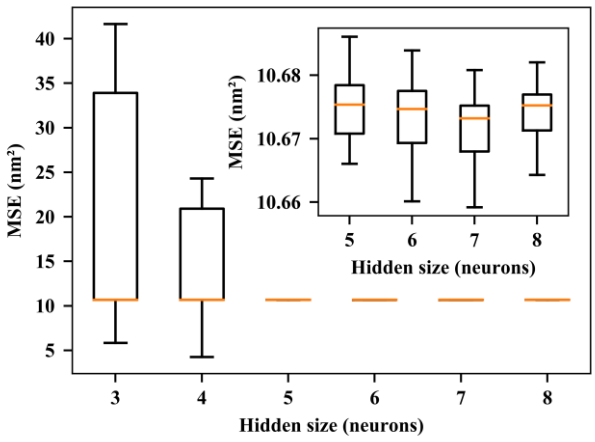

Fig. 7. Relationship between hidden layer size (number of neurons) and validation mean squared error for the 20 experiments per configuration.

diagonal indicated that each FBG contributed equally to the LPG resonant wavelength information extraction. Moreover, the darker diagonal in Fig. 5b is thicker than the Fig 5a. diagonal. The thicker diagonal indicates that there are more FBGs in the LPGs' dip; therefore, more spectral information is retrieved by the 1512 nm – 1584 nm FBG array. Fig. 6 shows the designed 1512 nm – 1584 nm FBG array alongside an LPG spectrum; note how the FBGs filter the LPG dip to extract information on the resonant wavelength position

The 20 tests per hidden layer configuration are summarized in Fig. 7 by a boxplot. We observed five neurons are sufficient for estimating the LPG resonant wavelength, we can see in Fig. 7 that the mean MSE during the 20 tests remained almost the same for all tested configurations, but the maximum and minimum MSE fluctuated severely for a hidden size of 3 and 4 neurons. Therefore, we choose the smaller hidden layer that didn't present such high fluctuation; hence the final MLP has five neurons in its hidden layer.

Finally, the designed interrogator was: an FBG filter array with 13 equally spaced FBGs from 1512 nm to 1584 nm, a preprocessing step that normalizes the array power to [0,1] range, and a 13x5x1 MLP that outputs the LPG resonant wavelength. The trained MLP can be implemented using the matrices

$$B_H = \begin{bmatrix} 61.793 & -0.431 & 4.116 & -0.334 & 62.549 \end{bmatrix}$$

$$W_h = \begin{bmatrix} 4.818 & 0.298 & -7.748 & -0.526 & 1.964 \\ 1.479 & 0.527 & -3.497 & -0.474 & 1.129 \\ 2.021 & -0.135 & -3.687 & -0.101 & 0.180 \\ 2.099 & -0.242 & -3.502 & 0.419 & -0.460 \\ 2.128 & -0.159 & -3.300 & 0.045 & -1.024 \\ 1.277 & 0.015 & 3.044 & 0.354 & -0.656 \\ 1.424 & -0.466 & -3.411 & -0.033 & -0.929 \\ 1.115 & -0.218 & -2.058 & 0.227 & -0.909 \\ 1.128 & 0.191 & 2.683 & -0.161 & -2.424 \\ 0.336 & 0.233 & 4.333 & -0.530 & -1.860 \\ 0.560 & -0.274 & 4.238 & -0.301 & -2.300 \\ 0.056 & -0.488 & 5.239 & -0.385 & -1.959 \\ 0.332 & -0.264 & 5.523 & -0.468 & -3.555 \end{bmatrix}$$

$$W_y = \begin{bmatrix} 12.767 \\ 0.337 \\ 10.221 \\ -0.424 \\ 10.577 \end{bmatrix}$$

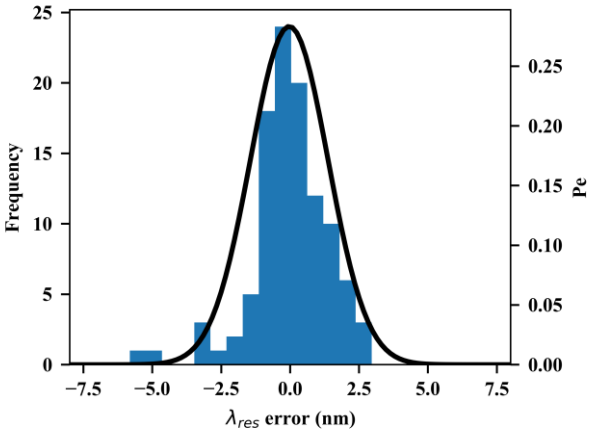

Fig. 9. Residuals histogram (left y-axis) and its parametric fit to a normal distribution (right y-axis).

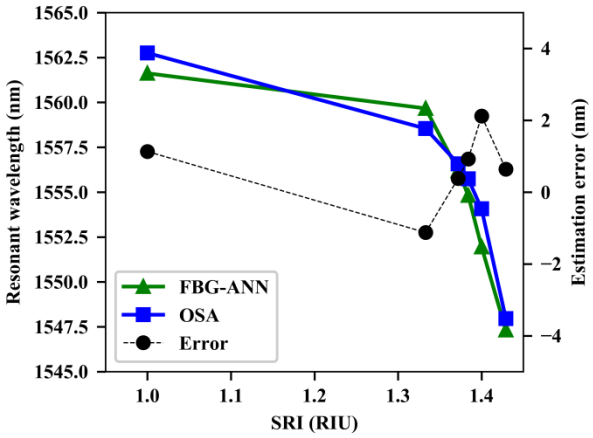

Fig. 10. SRI measurements using the proposed interrogator (left y-axis). The results obtained by an OSA are presented for comparison and the error is displayed at the right y-axis.

$$b_y = 10.185$$

and the matrix notation of eqs. (2) and (3):

$$H = f(B_h + W_h \cdot X) \quad (4)$$

$$y = b_y + W_y \cdot H \quad (5)$$

We estimated the interrogator MSE as 1.98 nm² and the MAE as 1.00 nm, using the test data. In Fig 8 the visual overview of the proposed interrogator performance can be seen. The perfect interrogator is the curve represented by the solid black line in Fig 8. The red dots are the results obtained for the proposed interrogation technique. One can see that we obtained a reasonable approximation for λ_{res}, since the red dots follow the solid line closely. Indeed, we obtained R2 = 0.993 for the proposed interrogator, indicating that the MLP model explained very well the observed data.

The difference between the red data points and the black line represents the λ_{res} estimation residuals; the distribution of the residuals is shown in Fig. 9. We fitted a Gaussian distribution to residuals histogram to obtain the error probability function (Pe), shown in Fig. 9 right y-axis.

The mean value for this normal distribution is μ = -0.0330 nm and its standard deviation is σ = 1.41 nm. Therefore the proposed interrogator could estimate an LPG resonant wavelength with -33.0 pm bias and 2.82 nm uncertainty, considering a 95% confidence interval.

In [13] three thermally modulated fiber-coupled laser diodes were used to scan the LPG spectrum and reconstruct it by fitting functions. The authors showed this curve fitting approach could estimate the LPG resonant wavelength in the 1530 nm – 1570 nm region within 1.12 nm error. But the approximation function needed to be refitted for each LPG used.

In this study, we showed incorporating machine learning in a similar but simpler setup increased the interrogator generalization. The proposed interrogator was able to estimate the resonant wavelength with 1.00 nm MAE without LPG-dependent refitting and filter modulation. Furthermore, our proposal obtained an error distribution with μ = -0.0330 nm and σ = 1.41 nm for 106 spectra from different LPGs in the 1510 nm – 1585 nm region, which is almost double the dynamic range reported in [13] and three times the dynamic range reported in [12], which used a much more complex setup: a 32 channel thermally modulated AWG with subnanometric channel spacing. Therefore, our approach to low-cost LPG interrogation obtained a similar resolution to the dynamic range ratio as reported in [13].

Fig. 10 shows the surrounding refractive index characterization of a 340 µm period LPG using the proposed FBG-ANN interrogator (green triangles) and using an OSA (blue squares) for comparison. The left y-axis shows the measured resonant wavelength and the right y-axis shows the error obtained by the FBG-ANN interrogator, using the OSA measurements as a baseline.

One can see that the FBG-ANN interrogator correctly estimates the LPG behavior under refractive index changes. The maximum absolute error was 2.12 nm and the MAE 1.05 nm, which are values close to the previously estimated for the interrogator's confidence interval and MAE, respectively. Furthermore, besides the high error, the interrogator response was linear and the results for refractive index measurements followed the expected. Thus, the proposed interrogator could be implemented for in-field measurements with proper calibration.

IV. Conclusion

This work proposes an LPG interrogator in a very generic form, i.e. the interrogation is LPG-independent. Our proposal used an FBG filter array to extract spectral information and an MLP to process this information and estimate the LPG resonant wavelength. We demonstrated the filter array design, the MLP selection, training, and evaluation over a wide range of LPGs.

The new approach to LPG resonant wavelength estimation is promising, the proposed interrogator is capable of estimating the LPG λ_{res} with 1510 nm to 1585 nm dynamic range with 2.82 nm uncertainty, despite any prior information on the LPG spectra. The total cost of the interrogator's optical components might be around US$ 3.000. We estimated this value based on the cost of approximately US$ 50 for a 1x16 PLC fiber optic splitter, US$ 50 for each fiber coupled photodiode (final price could be reduced if photodiode arrays are used, which costs around US$ 300 for an 8-ch device), US$ 150 for each optical circulator, and US$ 400 for the FBG array.

We showed an application of the proposed interrogator by using it to measure SRI from 1.000 RIU to 1.429 RIU and the obtained error was within the estimated uncertainty, furthermore, the resonant wavelength detection was linear, without hysteresis.

Furthermore, our proposal can be tailored for different dynamic ranges, i.e. for LPGs working over any window of the optical spectrum. Multiple LPGs could also be interrogated by time-division multiplexing (TDM) using optical switches.

Further investigation on the relationship between FBG spacing and the interrogator uncertainty is valuable to give the designer more control over the final LPG interrogator and proper adjustment to desired resonant wavelength resolution.

Since our database was composed of only single peak LPGs, the investigation on dual peak LPGs is also valuable; for this, a data set containing several dual peak LPGs could be used to train the ANN to estimate two peaks, thus increasing the model and database complexity. Alternatively, the dual peak LPG input data could be preprocessed using an attention mechanism to perform some sort of wavelength division multiplexing, showing each peak individually to the ANN; therefore, the ANN still identifies only one peak, resulting in a simpler model and dataset. The same approach could also be done for multiple single peak LPG sensors as an alternative to TDM.

REFERENCES

[1] J. L. Santos and F. Farahi, *Handbook of optical sensors*, 1st ed. CRC Press, 2014.

[2] G. Rego, P. Marques, J. Santos, and H. Salgado, "Arc-induced long-period gratings," *Fiber and Integrated Optics*, vol. 24, no. 3-4, pp. 245-259, 2005.

[3] A. M. Vengsarkar, P. J. Lemaire, J. B. Judkins, V. Bhatia, T. Erdogan, and J. E. Sipe, "Long-period fiber gratings as band-rejection filters," *Journal of lightwave technology*, vol. 14, no. 1, pp. 58-65, 1996.

[4] T. Erdogan, "Fiber grating spectra," *Journal of Lightwave Technology*, vol. 15, no. 8, pp. 1277-1294, 1997.

[5] X. Shu, L. Zhang, and I. Bennion, "Sensitivity characteristics of long-period fiber gratings," *Journal of Lightwave Technology*, vol. 20, no. 2, pp. 255-266, 2002.

[6] B. C. Lee, E.-J. Jung, C.-S. Kim, and M. Y. Jeon, "Dynamic and static strain fiber Bragg grating sensor interrogation with a 1.3 μm fourier domain mode-locked wavelength-swept laser," *Measurement Science and Technology*, vol. 21, no. 9, p. 094008, 2010.

[7] J. Park, Y. S. Kwon, M. O. Ko, and M. Y. Jeon, "Dynamic fiber bragg grating strain sensor interrogation based on resonance fourier domain mode-locked fiber laser," in *Avionics and Vehicle Fiber-Optics and Photonics Conference (AVFOP), 2016 IEEE*. IEEE, 2016, pp. 291-292.

[8] H. Patrick, G. Williams, A. Kersey, J. Pedrazzani, and A. Vengsarkar, "Hybrid fiber Bragg grating/long period fiber grating sensor for strain/temperature discrimination," *IEEE Photonics Technology Letters*, vol. 8, no. 9, pp. 1223-1225, 1996.

[9] T. Allsop, T. Earthrowl, R. Reeves, D. J. Webb, and I. Bennion, "The interrogation and multiplexing of long period grating curvature sensors using a bragg grating based, derivative spectroscopy technique," *Measurement Science and Technology*, vol. 15, no. 1, p. 44, 2003.

[10] J. Carvalho, L. Coelho, M. Pontes, A. Barbero, M. Martinez, R. Ribeiro, J. Weyl, J. Baptista, M. Giraldi, I. Dias *et al.* "Long-period gratings dynamic interrogation with modulated fiber bragg gratings and optical amplification," *IEEE Sensors Journal*, vol. 12, no. 1, pp. 179-183, 2011.

[11] G. Kahandawa, J. Epaarachchi, H. Wang, D. Followell, and P. Birt, "Use of fixed wavelength Fibre-Bragg Grating (FBG) filters to capture time domain data from the distorted spectrum of an embedded fbg sensor to estimate strain with an artificial neural network," *Sensors and Actuators A: Physical*, vol. 194, pp. 1-7, 2013.

[12] H. Guo, G. Xiao, N. Mrad, and J. Yao, "Interrogation of a long-period grating sensor by a thermally tunable arrayed waveguide grating," *IEEE Photonics Technology Letters*, vol. 20, no. 21, pp. 1790-1792, 2008.

[13] P. S. dos Santos, P. A. Jorge, J. M. de Almeida, and L. Coelho, "Low-cost interrogation system for long-period fiber gratings applied to remote sensing," *Sensors*, vol. 19, no. 7, p. 1500, 2019.

[14] J. Sun, C. Chan, K. Tan, X. Dong, and P. Shum, "Application of an artificial neural network for simultaneous measurement of bending curvature and temperature with long period fiber gratings," *Sensors and Actuators A: Physical*, vol. 137, no. 2, pp. 262-267, 2007.

[15] J. Sun, C. Chan, X. Dong, and P. Shum, "Application of an artificial neural network for simultaneous measurement of temperature and strain by using a photonic crystal fiber long-period grating," *Measurement Science and Technology*, vol. 18, no. 9, p. 2943, 2007.

[16] R. Costa, G. Possetti, L. De Arruda, M. Muller, and J. Fabris, "Curvature vector smart sensing with a long-period fibre grating probed by artificial intelligence," *Measurement Science and Technology*, vol. 21, no. 9, p. 094027, 2010.

[17] F. Barino, F. Delgado, M. A. Jucá, T. V. Coelho, and A. B. dos Santos, "Comparison of regression methods for transverse load sensor based on optical fiber long-period grating," *Measurement*, vol. 146, pp. 728-735, 2019.

[18] G. Possetti, L. Côcco, C. Yamamoto, L. De Arruda, R. Falate, M. Muller, and J. Fabris, "Application of a long-period fibre grating-based transducer in the fuel industry," *Measurement Science and Technology*, vol. 20, no. 3, p. 034012, 2009.

[19] X. Hu, H. Si, H. Shen and Z. Yu, "A fuzzy neural network model to determine axial strain measured by a long-period fiber grating sensor", *Measurement and Control*, p. 002029401990130, 2020.

[20] M. Al-Tarawneh, Y. Huang, P. Lu and D. Tolliver, "Vehicle Classification System Using In-Pavement Fiber Bragg Grating Sensors," *IEEE Sensors Journal*, vol. 18, no. 7, pp. 2807-2815, 1 April1, 2018,

[21] M. A. Kamizi, G. R. C. Possetti, M. Muller, and J. L. Fabris, "Fiber Bragg grating sensors probed by artificial intelligence to detect and localize impacts on structures", *JMOE*, vol. 14, p. SI-25 to SI, Aug. 2015

[22] L. Shiloh, A. Eyal and R. Giryes, "Deep Learning Approach for Processing Fiber-Optic DAS Seismic Data", *26th International Conference on Optical Fiber Sensors*, 2018.

[23] M. Basu and S. Ghorai, "Sequential interrogation of multiple FBG sensors using LPG modulation and an artificial neural network", *Measurement Science and Technology*, vol. 26, no. 4, p. 045104, 2015.

[24] Mei Nar Ng, Zhihao Chen and Kin Seng Chiang, "Temperature compensation of long-period fiber grating for refractive-index sensing with bending effect", *IEEE Photonics Technology Letters*, vol. 14, no. 3, pp. 361-362, 2002.

[25] C. Trono, F. Baldini, M. Brenci, F. Chiavaioli and M. Mugnaini, "Flow cell for strain- and temperature-compensated refractive index measurements by means of cascaded optical fibre long period and Bragg gratings", *Measurement Science and Technology*, vol. 22, no. 7, p. 075204, 2011.

[26] Y. Wang, L. Xiao, D. Wang and W. Jin, "Highly sensitive long-period fiber-grating strain sensor with low temperature sensitivity", *Optics Letters*, vol. 31, no. 23, p. 3414, 2006.

[27] P. K. Simpson, *Artificial Neural Systems Foundations, Paradigms, Applications, and Implementations*. McGraw-Hill, New York, 1990.
[28] D. W. Patterson, *Artificial neural networks: theory and applications*. Prentice Hall PTR, 1998.
[29] K. Hornik, M. Stinchcombe, and H. White, "Multilayer feedforward networks are universal approximators," *Neural networks*, vol. 2, no. 5, pp. 359-366, 1989.
[30] L. Buitinck, G. Louppe, M. Blondel, F. Pedregosa, A. Mueller, O. Grisel, V. Niculae, P. Prettenhofer, A. Gramfort, J. Grobler, R. Layton, J. VanderPlas, A. Joly, B. Holt, and G. Varoquaux, "API design for machine learning software: experiences from the scikit-learn project," in *ECML PKDD Workshop: Languages for Data Mining and Machine Learning*, 2013, pp. 108-122.

Felipe O. Barino was born in Juiz de Fora, Brazil, in 1996. He received his B.S. degree in electronics from the Federal University of Juiz de Fora (UFJF), Minas Gerais, Brazil, in 2019 and is now pursuing his M.S. degree in electrical engineering at Programa de Pós Graduação em Engenharia Elétrica - PPEE/UFJF. His current research interests are related to instrumentation, optical fiber sensors, and machine learning.

Alexandre Bessa dos Santos was born in Juiz de Fora, Brazil, in 1975. He received the M.S. and Ph.D. degrees in electrical engineering from Pontifical Catholic University (PUC), Brazil, in 2001 and 2005, respectively. Since 2010, he has been an Associated Professor with the Department of Circuits at Federal University of Juiz de Fora (UFJF), Juiz de Fora. His research interests include applied electromagnetism, optical sensors, computational methods, instrumentation, and metrology.